Fission fragment mass yield deduced from density distribution in the pre-scission configuration

2015 Phys. Scr. 90 114003

(http://iopscience.iop.org/1402-4896/90/11/114003)

IOP Publishing | Royal Swedish Academy of Sciences Physica Scripta

Phys. Scr. **90** (2015) 114003 (10pp) doi:10.1088/0031-8949/90/11/114003

Fission fragment mass yield deduced from density distribution in the pre-scission configuration

M Warda and A Zdeb

Department of Theoretical Physics, Maria Curie-Skłodowska University, Lublin, Poland

E-mail: warda@kft.umcs.lublin.pl

Received 17 November 2014, revised 17 May 2015
Accepted for publication 1 June 2015
Published 29 October 2015

Abstract

Static self-consistent methods usually allow one to determine the most probable fission fragments mass asymmetry. We have applied random neck rupture mechanism to the nuclei in the configuration at the end of fission paths. Fission fragment mass distributions have been deduced from the pre-scission nuclear density distribution obtained from the self-consistent calculations. Potential energy surfaces as well as nuclear shapes have been calculated in the fully microscopic theory, namely the constrained Hartree–Fock–Bogoliubov model with the effective Gogny D1S density-dependent interaction. The method has been applied for analysis of fission of ^{256,258}Fm, ^{252}Cf and ^{180}Hg and compared with the experimental data.

Keywords: nuclear fission, fragment mass distribution, scission point

(Some figures may appear in colour only in the online journal)

1. Introduction

Fission is one of the dominant decay channels of the heaviest nuclei. Physics of this process is crucial in determining stability of heavy and super-heavy isotopes. One of the basic observables of fission, obtained directly in experiment, is fragment mass distribution. Measured yields allow one to determine the type of fission as well as to deduce the properties of the mother nucleus. Prediction of the charge, mass and total kinetic energy (TKE) distributions of fission fragments is still a challenging task for the theory of nuclear fission. A number of attempts have been made to describe the mechanism of sharing nucleons between fission fragments since the spontaneous fission phenomenon was discovered.

Historically, in the first theoretical description of fission the macroscopic liquid drop model was used. In this approach the competition between Coulomb repulsion and surface energy of deformed charged liquid drop of nuclear matter is analyzed. The mass distributions calculated within this method are symmetric, as a consequence of ignoring microscopic effects, that are responsible for octupole deformation of mother nucleus and deformations of the fragments [1]. The more sophisticated approach, scission point model [2], assumes that fission properties can be derived from the scission point configuration that is well defined in the evolution of fissioning nucleus. The scission point is described as a configuration of two deformed touching fragments. The potential energy is calculated using macroscopic–microscopic model. The probability of certain fragmentation is in inverse proportion to the scission point potential energy. This method allows one to determine the probability, that the certain number of nucleons will be incorporated into one of the fragments from the energy of the scission configuration.

Within improved scission point model [3–5] one can obtain distribution of fission fragments and the mean value of TKE. In comparison to [2] this model allows one to calculate the energy of interaction between fragments and deformation energy at the scission point configuration, which results in obtained mass and TKE distributions. The main disadvantage of this treatment is a large number of phenomenological parameters, e.g. touching distance of fissioning system, surface tension coefficient with parameters fitted to the magic nuclei.

The authors of the microscopic scission point method [6] also deduce fission properties as fragment mass and TKE from the analysis of dinuclear system that may be created

after scission. Energies of nuclei are obtained in the microscopic self-consistent calculations. Depending on mass asymmetry and deformation of the fragments, the energy of the system is calculated and fission probability is determined. In this approach, strong assumptions on distance between fragments and deformation of the fragments at scission point have to be made.

Another approach includes dynamics of fission in the analysis. It treats the nuclear shape evolution as a Brownian motion of nuclear system on the potential energy surface (PES) [7, 8]. The direction of the motion in the five-dimensional deformation space is determined randomly using Metropolis' method. The considered PES is calculated within the macroscopic–microscopic model, where the potential energy consists of liquid drop part (with deformation-dependent coefficients) and microscopic corrections. During a 'random walk' on this surface each shape might be obtained with accordance to its statistical weight. The dimensional depletion causes agreement with experimental mass distribution to get worse. The additional parameter—critical neck radius was introduced, and its value results much from the obtained fragment mass yields.

There were also several attempts to describe fragment mass distribution in a fully microscopic way, i.e. using Gaussian overlap approximation (GOA) of the time-dependent generator coordinate method (GCM) [9] or Hartree–Fock–Bogoliubov (HFB) method with Skyrme energy functional [10]. The GCM+GOA approach allows one to include dynamical effects on the description of the fission process. The probability of mass division is proportional to the total flux of the wave function through the scission point in a particular configuration. Including dynamic effects gives much better agreement with data in comparison with static calculations. Especially, the broadness of fragment mass distribution is closer to the experimental one.

The same formalism (GCM+GOA) was recently applied to describe low energy fission [11]. The mass and TKE distributions were calculated and compared to the experimental data.

The HFB method with Skyrme energy functional was applied for description of the induced fission process [10]. The authors discussed the impact of the triaxiality and discontinuity of the PES in the scission point region on the fragment mass distribution. Quasi-particle occupations in the nascent fragments were localized and attributed to each fragment.

Dynamic calculations at low excitation energy were performed using Langevin approach [12]. Shell and pairing effects, as well as dissipation and fluctuation were included in the model. Out of fragment mass distribution it was also possible to obtain the time scale of fission process. The authors made a strong assumption, that both nascent fragments have the same deformation, which argues against several observations of shapes of fission products [13].

Published lastly, GEF code [14] predicts surprisingly good fission fragment mass yields with a very simple construction of the PES of fissioning nucleus. Namely, macroscopic potential is modified by parabolic corrections to simulate shell effects. Once fitted it reproduces a wide range of experimental fission results.

The main inspiration for our investigations is the idea proposed by Brosa *et al* [15–17]. The authors assume direct dependence of fragment mass distribution on the random neck rupture mechanism of mother nucleus in its pre-scission shape. The method describes splitting of a nucleus as a consequence of hydrodynamic fluctuations induced by random vibrations of the nuclear surface. The pre-scission deformation of the fissioning nucleus has a decisive influence on the fragment mass yield. The probability, that the rupture of the neck occurs in a certain position, decreases with the radius of a neck. In this method no assumption on properties of fission fragments is needed. This simple macroscopic model, allows one to describe many fission properties such as the TKE distribution and the dependence of neutron multiplicity on fragment masses.

We apply the HFB model, employing finite-range Gogny forces to calculate the PES and mass distribution during fission. The previous investigations performed with this model have proven that it describes with reasonable accuracy the experimental data of the most relevant properties of unstable nuclei for different decay modes, such as spontaneous [18–20] and induced [21] fission, and the exotic process of cluster radioactivity [23]. Also, the asymmetric fission of ^{180}Hg isotope was successfully explained within the microscopic approach [24]. In this paper detailed analysis of the scission point configuration determined in the microscopic calculations is performed. From the single mass distribution we deduce possible fragment mass asymmetries.

This paper is constructed as follows: in the second section details of calculations are described. Results obtained for four isotopes are presented in the third section. Finally, the fourth section includes our conclusions and discussion of the results.

2. Method

The analysis of the scission point configurations requires realistic description of the nuclear matter mass distributions at large deformations. They may be provided by the calculations performed within the self-consistent constrained HFB model with the effective Gogny density-dependent interaction [26]. The popular D1S parametrization [27] was used. The computer code of [28] was applied for numerical calculations. The PES was determined in the deformation space of quadrupole and octupole deformations. In the PES the fission paths were determined as continuous lines connecting local minima of energy for fixed value of quadrupole moment. In each point of the constrained calculations nuclear matter spatial distribution can be easily derived from the single-nucleon wave functions.

2.1. The pre-scission point configuration

The scission point is defined as the configuration of the nuclear system in which molecular shape (i.e. two fragments connected by a thin neck) of a mother nucleus converts into two separate

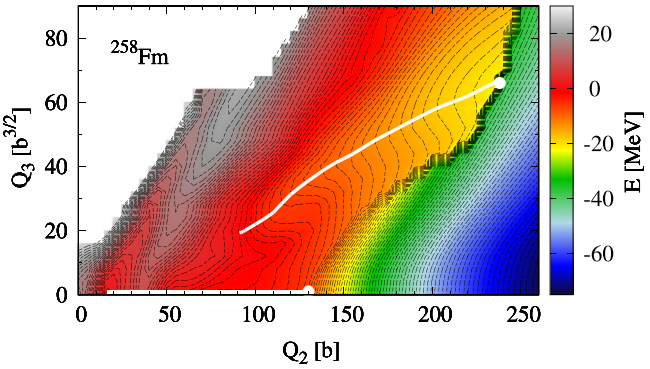

Figure 1. The PES of ^{258}Fm. The white lines correspond to the fission paths.

fragments. In some simple models it is represented by the configuration of two touching nascent nuclei. In fact, when a realistic leptodermous density distribution is taken into account, one can find that during the splitting nuclear matter, density in the neck decreases gradually from the bulk value to zero, while surfaces of the fragments overlap. Thus we cannot define one scission configuration, but rather a scission region in which two fragments are being separated.

In the self-consistent calculations of the PES it is easy to locate the ranges of the scission region. Increasing constraint on deformation parameter, e.g. quadrupole moment, leads to more elongated shape of a nucleus with a thinner neck. At some point sudden change takes place. The energy minimization procedure leads not to molecular shape, but a solution with two nuclei separated by a few fm distance is found. Such a dinuclear system usually has energy much lower than the compound nucleus calculated in the previous step. Surely, scission take place between these two configurations. In this way the last point on the fission valley before rupture should be called pre-scission point and the next point with two separated fragments post-scission point. The line connecting pre-scission points on the PES should be called scission line (or more precisely pre-scission line), see figure 1. The binuclear configuration beyond scission line, obtained in the self-consistent calculations with constraints on quadrupole and octupole moments, corresponds to its pre-scission neighbour. Fragment mass asymmetry is not more than a few nucleons different from the asymmetry of the molecular shape split in the thinnest neck. Nevertheless, nuclear matter distribution and deformation of the fragments are very distinct in both cases and more careful studies should be made to determine the post-scission configuration [6, 29, 30]. Intermediate configurations of the scission region are hard to obtain in the self-consistent procedure, as they require multiple constraints, including e.g. neck parameter [23, 24].

The evolution of shape along fission path goes smoothly with increase of deformation up to the pre-scission point. It was found [18, 24], that many fission properties are determined by the shape of the PES from saddle to scission, where a nucleus takes a molecular shape. Especially the configuration in the pre-scission point is crucial in the fission process as no further evolution of a compound nucleus is allowed.

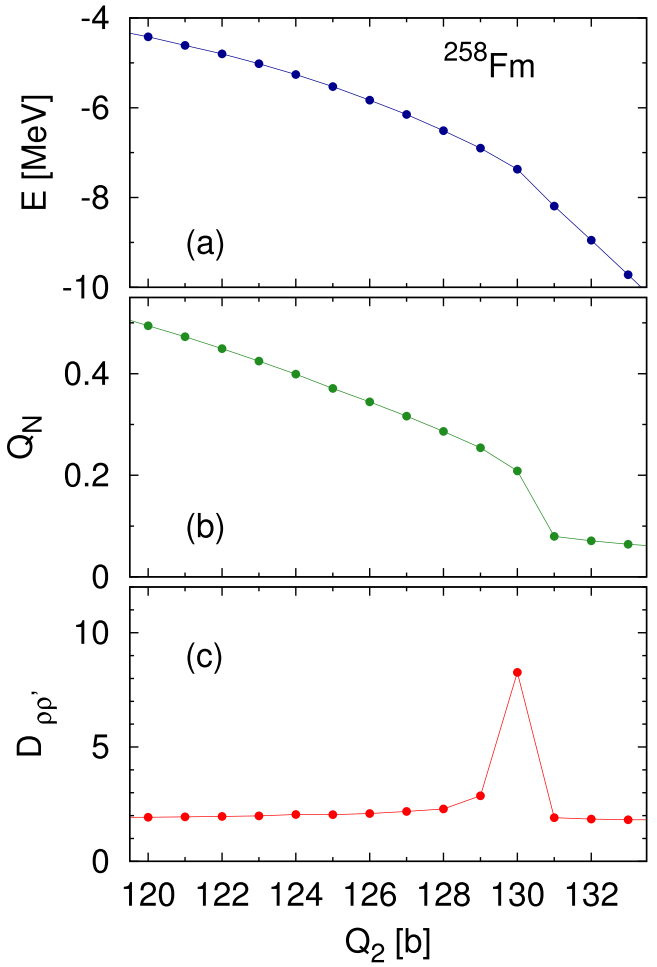

Figure 2. The fragment of the compact fission path of ^{258}Fm in the vicinity of scission point. (a) The energy, (b) the neck parameter Q_N and (c) the density distance function $D_{\rho\rho'}$ between two neighbouring configurations as a function of the quadrupole moment Q_2.

In most cases determination of the scission line is trivial, as in the constrained calculations many observables essentially change their values: e.g. energy, hexadecapole moment, neck thickness. Such a line can be easily noticed in figure 1 between $Q_2 = 130$ b and 250 b as rapid change of energy of the system takes place along scission line.

In the case of symmetric fission path in ^{258}Fm at $Q_3 = 0$ b$^{3/2}$ it is not so clear as molecular shape converts quite smoothly into the dinuclear system without a sudden drop of energy. It can be easily found in the panel (a) of figure 2, where fission path smoothly converts into hyperbolic decrease characteristic for Coulomb repulsion between separated fragments. Thus fall of energy cannot be a criterion to determine the scission point. Detailed calculations show only a tiny kink with change of energy derivative when the neck is about to disappear. To prove that this is the real scission point, first we calculate neck parameter Q_N defined as:

$$Q_N = \int \rho\left(z, r_\perp\right) \exp\left(\frac{z^2}{a_0^2}\right) \mathrm{d}z\mathrm{d}r_\perp, \qquad (1)$$

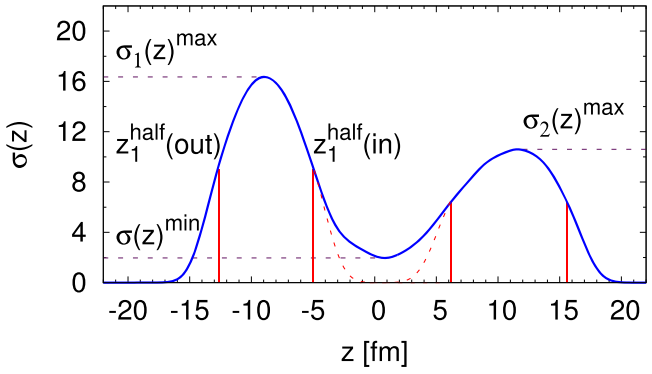

Figure 3. Linear density of ^{258}Fm in its pre-scission shape.

where a_0 is a parameter describing width of a neck region with an arbitrary chosen value $a_0 = 1$ fm. Q_N describes the number of particles in the neck region. The middle panel of figure 2 shows changes of a neck parameter along the fission path. In the first part of the fission path Q_N decreases slowly, whereas beyond $Q_2 = 129$ b it drops down rapidly. It means that a sudden change in density distribution takes place here. Neck parameter takes small positive and almost constant values from $Q_2 = 130$ b. This is characteristic behaviour of Q_N for two separated nuclei when only tails of density distribution of both fragments contribute to Q_N.

As was mentioned, scission point may be defined as a configuration, where rapid change of matter distribution from molecular to dinuclear system occurs. To check discontinuity in changes of density of nucleons it is useful to follow the procedure of [31]. We may define the density distance function $D_{\rho\rho'}$ given by:

$$D_{\rho\rho'} = \int \left|\rho(\mathbf{r}) - \rho'(\mathbf{r})\right| \mathrm{d}\mathbf{r}, \tag{2}$$

where $\rho(\mathbf{r})$ and $\rho'(\mathbf{r})$ are the the local spatial densities, calculated in two following steps during the nuclear shape evolution. This function takes small values during smooth evolution of nuclear shape. When two different configurations are compared it is manifested by a sharp single peak.

In the panel (c) of figure 4 we can find again that function $D_{\rho\rho'}$ is four times larger at $Q_2 = 130$ b in comparison to the neighbouring deformations. We can deduce rapid change of configuration between solutions at $Q_2 = 129$ b and at $Q_2 = 130$ b, namely rupture of the neck is observed.

All above-mentioned arguments show that at $Q_2 = 129$ b pre-scission point can be found on the symmetric fission path of ^{258}Fm.

2.2. Random neck rupture mechanism

It was proven in [24, 25] that the structure and basic properties of the nascent fragments are preliminarily determined in the pre-scission configuration of fissioning nucleus. In the pre-scission point two fragments are already created in the form of two nuclei connected by a neck.

The mass numbers A_1 and A_2 of fragments in molecular configuration before scission may be obtained in the simple procedure. First, one has to determine linear density of a

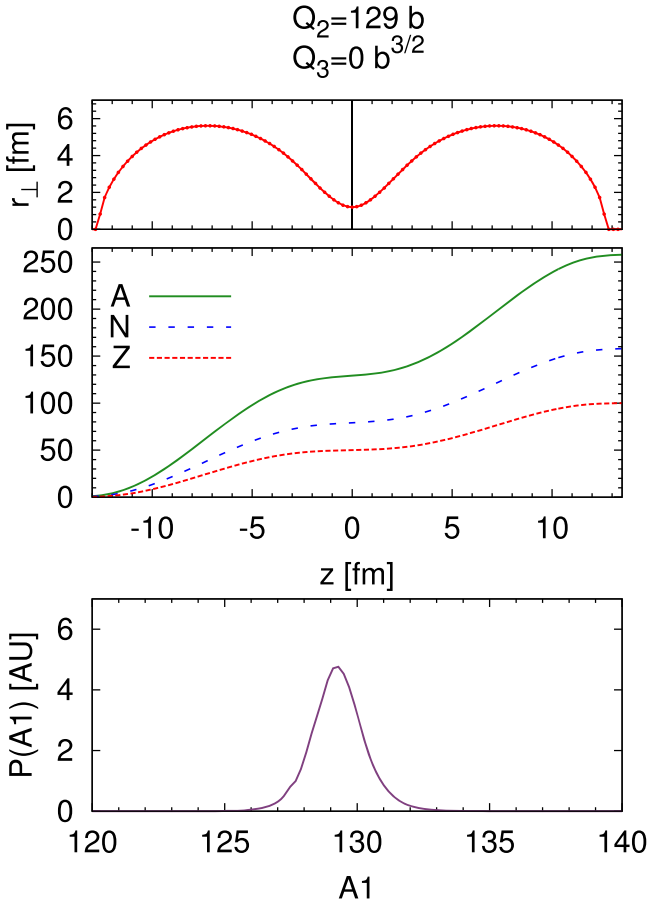

Figure 4. The upper panel shows the shape of the ^{258}Fm at a density of $\rho_0 = 0.08$ fm^{-3} in the pre-scission point on the symmetric path. The number of nucleons as a function of symmetry axis z (middle panel) and the probability of division of nucleons between nascent fragments, depending on the cross section of the neck in a certain position calculated using equation (7) (lower panel).

nucleus:

$$\sigma(z) = 2\pi \int_0^\infty r_\perp \rho(z, r_\perp) \mathrm{d}r_\perp, \tag{3}$$

where $\rho(z, r_\perp)$ is the spatial density of nuclear matter. Referring to figure 3, the positions z_i^{half} indicate the average value between $\sigma_i^{\max}$ in the fragment and $\sigma^{\min}$ in the neck. There are two points, that fulfill this condition for each fragment: inner ($z_{i,\mathrm{in}}^{\mathrm{half}}$) and outer ($z_{i,\mathrm{out}}^{\mathrm{half}}$). The sections of the nucleus between these points are well established central parts of the nascent fragments. The outer parts ($z < z_1^{\mathrm{half}}$(out) and $z > z_2^{\mathrm{half}}$(out)) also belong to the fragments. The central part of the pre-scission nucleus contains both the neck nucleons as well as nucleons associated with the each side of a nucleus. Therefore, to get the size of a fragment one has to simulate the inner tip of a fragment by the outer one (marked by dashed lines in figure 3) and integrate the volume of the pre-scission nucleus between $z_{i,\mathrm{out}}^{\mathrm{half}}$ and $z_{i,\mathrm{in}}^{\mathrm{half}}$ and double of the outer part. Numbers of neutrons and protons are the integers closest to the obtained values.

This method is similar to the scheme described in [24]. Most of the nucleons of the pre-scission configuration are

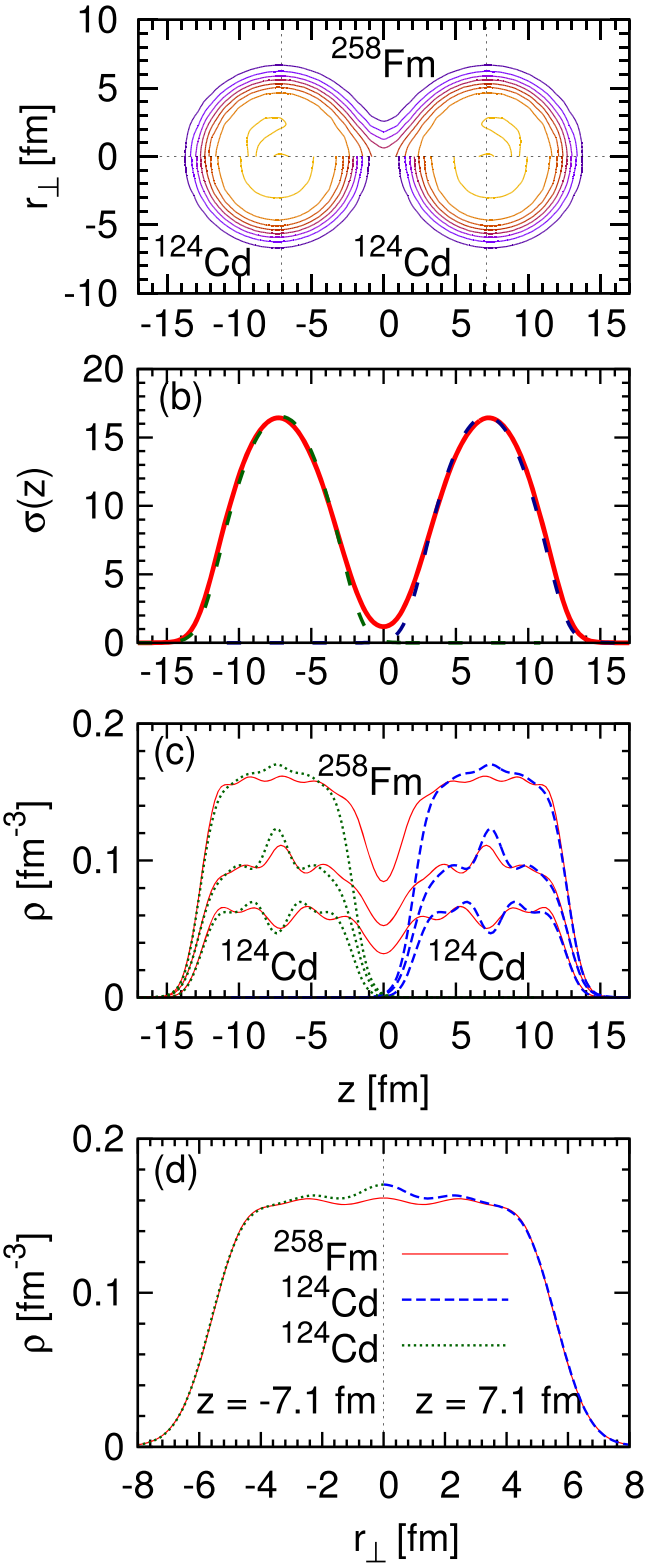

Figure 5. (a) Density distribution of ^{258}Fm in configuration close to the scission on the symmetric fission path (Q_{20} = 129 b, Q_{30} = 0 b$^{3/2}$) compared with the density distribution of ^{124}Cd (spherical shape). (b) Linear density of ^{258}Fm in its pre-scission shape (continuous line) and ^{124}Cd (dotted lines). Profiles of density for cross sections taken in (c) $r_\perp$ = 0 fm (total, neutron and proton density) and (d) $z = -7.1$ fm, z = 7.1 fm.

localized in the fragments, while a few of them (up to 20) create the neck. They will be incorporated to the nascent fragments during scission. Usually it is assumed, that the neck is ruptured in its thinnest place. In this way one can calculate how the neck nucleons are shared and the most probable mass asymmetry can be found.

Nevertheless, following the idea presented in [16, 17], the probability P of rupture of a neck depends on the energy $E_{\rm cut}$ needed to create a cut in the considered position z along the symmetry axis. For each position z we can calculate particular fragment mass asymmetry.

The probability P of the rupture of a neck, leading to fragment mass asymmetry A_1/A_2 reads:

$$P(A_1, A_2) \sim \exp(-E_{\rm cut}/T), \tag{4}$$

where $T = \sqrt{12E^{\rm sc}/A}$ is temperature of the pre-scission deformation. Excitation energy at scission:

$$E^{\rm sc} = E_{\rm g.s.} - E^{\rm sc}_{\rm def}, \tag{5}$$

which was gained during the evolution from the ground state to the pre-scission deformation. $E_{\rm cut}$ depends on the linear density $\sigma(z)$ of a neck in a position of z that corresponds to required fragment mass asymmetry. Note that two values of z give the same mass asymmetry but with lighter and heavier fragment placed at opposite sides. Cut energy is defined as:

$$E_{\rm cut}(z) = 2\gamma\sigma(z). \tag{6}$$

The expression for surface tension coefficient $\gamma = 0.9517[1 - 1.7826(1 - 2Z/A)^2]$ was taken from [32] and the linear density of a neck is given by equation (3). Finally, the probability for the rupture, with corresponding division of nucleons between fragments, takes the form:

$$P(A_1, A_2) = \exp[-2\gamma\sigma(z)/T]. \tag{7}$$

This method is visualized in figure 4, where the case of ^{258}Fm symmetric mode is considered. The top panel shows the shape of the nucleus at the half-bulk density $\rho = 0.08$ fm^{-3} in the pre-scission point [18]. Each neck's rupture position at the z axis is correlated with specific mass division between fragments shown in the middle panel of figure 4. The probability of the rupture decreases strongly, while the neck becomes thicker, according to equation (7). In consequence, mass yield presented in the lower panels of figure 4 is quite narrow with the most probable position of a rupture, corresponding to the equal split into two ^{129}Sn isotopes.

3. Results

It was shown, that fission in ^{258}Fm represents specific, bimodal character [33]. Its mass yield is very narrow with a single peak. The TKE distribution is compounded of the low and high energy modes with equal abundance. They can be linked to the theoretically described asymmetric and symmetric fission channels on the PES, respectively [18], which

are visible on the PES in figure 1. A nucleus in its ground state is quadrupole deformed ($Q_{20} = 16$ b). The symmetric path goes along reflection symmetric shapes and terminates at deformation close to $Q_{20} = 129$ b, as was discussed in the previous section. The density distribution corresponding to this pre-scission configuration is shown in the upper part of figure 5(a). The shape of a nucleus can be described as a molecular system of two spherical ^{124}Cd isotopes connected by a thin neck containing four protons and six neutrons. The fragments conserve N/Z ratio of mother nucleus and reproduce the shape and mass of the outer part of the fragments before scission. In panels (c) and (d) of figure 5 density profiles of ^{258}Fm and two ^{124}Cd are compared along z axis and along perpendicular axis at the thickest part of the fragments. Out of the neck region very good agreement can be noticed.

The alternative asymmetric path arises behind the barrier from $Q_{20} \approx 90$ b and $Q_{30} \approx 20$ b$^{3/2}$ and leads towards configuration close to $Q_{20} = 239$ b, $Q_{30} = 67$ b$^{3/2}$. The analysis of density profile of asymmetric pre-scission deformation is shown in figure 6(a). This molecular configuration consists of spherical double-magic ^{132}Sn and prolate ^{106}Mo. In this case, a neck contains eight protons and twelve neutrons. Again, in panels (c) and (d) of figure 6, nice reproduction of the density profiles of mother nucleus by nascent fragments can be found.

In the symmetric mode ten neck nucleons should be shared between fragments in the scission point. The most probable split of symmetric pre-scission shape leads to the production of two ^{129}Sn isotopes. In the asymmetric fission channel ^{143}Cs and ^{115}Rh isotopes are most likely created. If we assume, that neck does not have to be cut in the thinnest place, these numbers would convert into stretched fragment mass distribution. To this end the procedure presented in the previous section is applied twice, both for symmetric and asymmetric pre-scission shapes. From the density distribution linear density is calculated in each case, which can be seen in figures 5(b) and 6(b). Next, fission probability as a function of mass asymmetry is calculated from equation (7). The results are combined with assumption of equal abundance of both modes and plotted in figure 7 by a dotted line. In the same figure experimental results taken from [33] are shown. One can find that symmetric peak is much narrower than the experimental one. Asymmetric mode produces two additional side peaks at $A_H \approx 143$, $A_L \approx 115$ which are not visible in the experimental data. Nevertheless asymmetric peaks fit in the region of the tail of mass yield of ^{258}Fm.

The main reason of inconsistency is lack of dynamic effects in the present analysis. In the final part of evolution of a nucleus, the PES is quite soft in Q_3 direction and wide fission valleys are developed (see figure 1). Up to now we have focused only on two pre-scission configurations at the end of symmetric and asymmetric fission paths, but one may also consider other scission points, deviated from the energetically most favourable. Such configurations give fragment mass distributions slightly shifted in comparison to the one of the most probable mass fragment (see figure 8). Analysis of the potential energy along scission line as a function of the

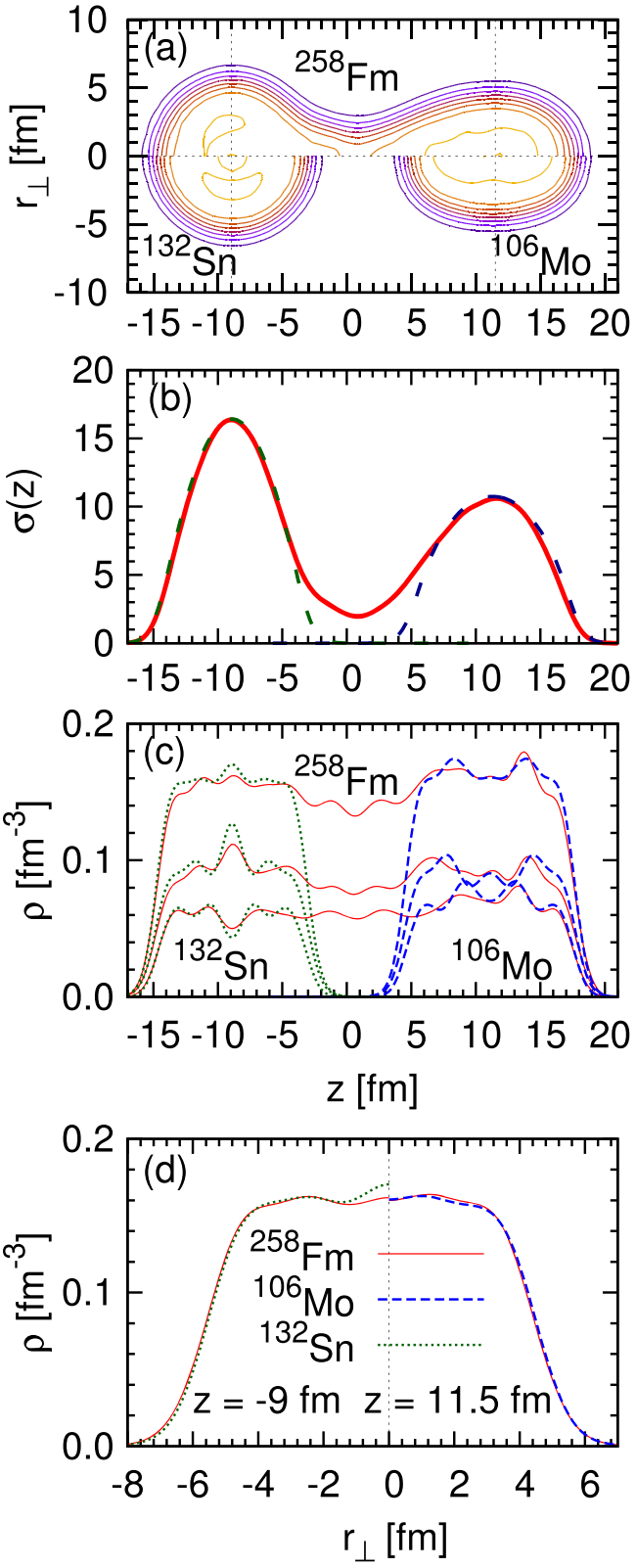

Figure 6. Similar as in figure 5 but for pre-scission configuration on asymmetric path ($Q_{20} = 238$ b, $Q_{30} = 66.7$ b$^{3/2}$). Density distribution and profiles are compared with ^{132}Sn (in its spherical ground state) and ^{106}Mo ($Q_{20} = 6$ b).

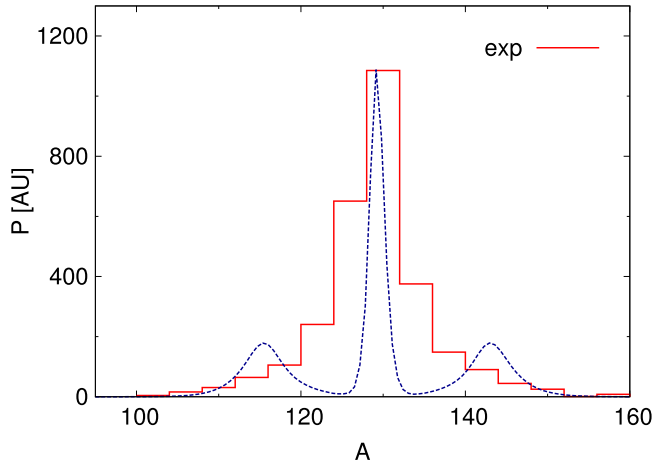

Figure 7. Fragment mass distribution for the spontaneous fission of ^{258}Fm obtained within presented method. The sum of distributions (dotted line), corresponding to the symmetric and asymmetric paths is compared with the experimental yield, taken from [33].

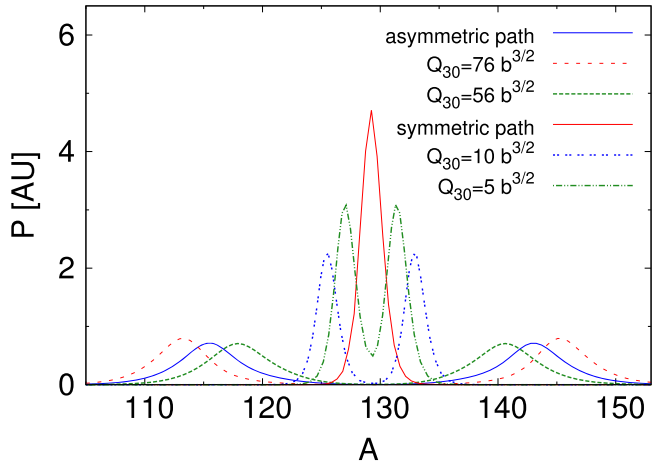

Figure 8. Fragment mass distributions deduced from the pre-scission configurations at the end of symmetric and asymmetric path (solid lines) and in neighbourhood (dashed lines).

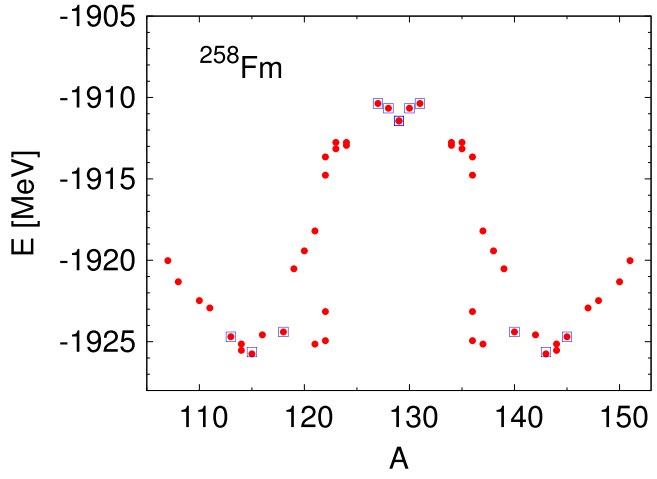

Figure 9. The potential energy of ^{258}Fm along the scission line as a function of the most probable fragmentation. The blue squares correspond to the distributions plotted in figure 8.

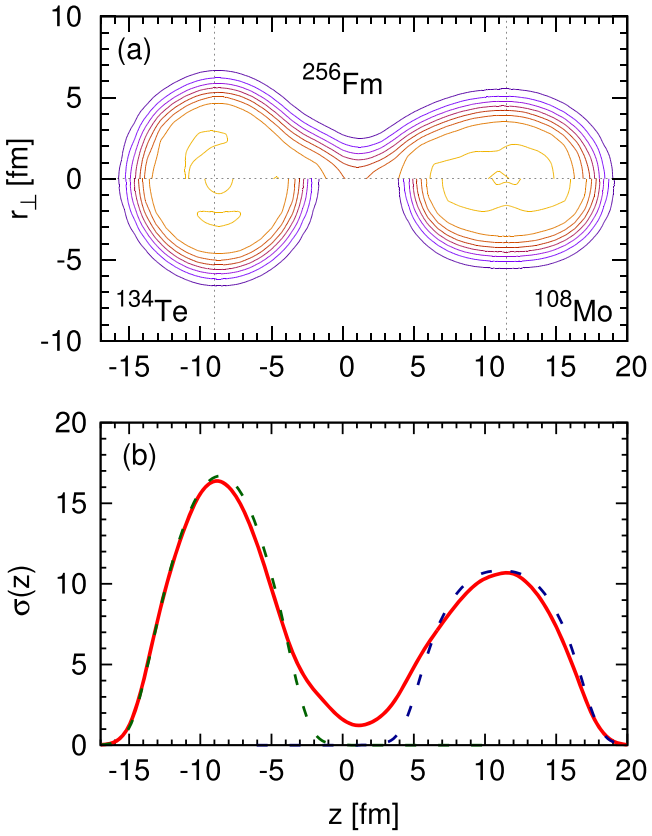

Figure 10. Similar as in figure 5 but for pre-scission configuration of ^{256}Fm (Q_{20} = 230 b, Q_{30} = 68 b$^{3/2}$). Density distribution and profiles are compared with ^{134}Te (Q_{20} = 1 b) and ^{108}Mo (Q_{20} = 6 b).

mass fragment (figure 9) shows that changes of energy are rather small in the close neighbourhood of these points, with non-negligible shifts of the most probable fragmentation. That is consistent with results presented in [11]. One may expect, that the probabilities of shape evolution towards these scission points should be comparable. Combining results along the whole scission line with weights corresponding to the probability of reaching given scission configuration should allow one to reproduce experimental data. The exact probability may be obtained in dynamical calculations described e.g. in [9]. From each pre-scission shape fragment mass distribution can be deduced. It is planned to involve a combination of these two effects in our future investigations, which should allow us to obtain broader mass yield.

The fission properties of ^{256}Fm differ substantially from its neighbour isotope with two more neutrons. Its spontaneous fission half-life is seven orders of magnitude longer and symmetric fission channel is not active. The detailed explanation of these facts can be found in [18]. In ^{256}Fm only the asymmetric channel of fission is visible in the experiment. Analysis of the density profile of the pre-scission configuration (figure 10) indicates that the nascent fragments are close to the ^{134}Te and ^{108}Mo with six protons and eight neutrons in a neck region. From the linear density function $\sigma(z)$ presented in figure 10(b) the fission fragment mass distribution are obtained within the presented method. The results are shown

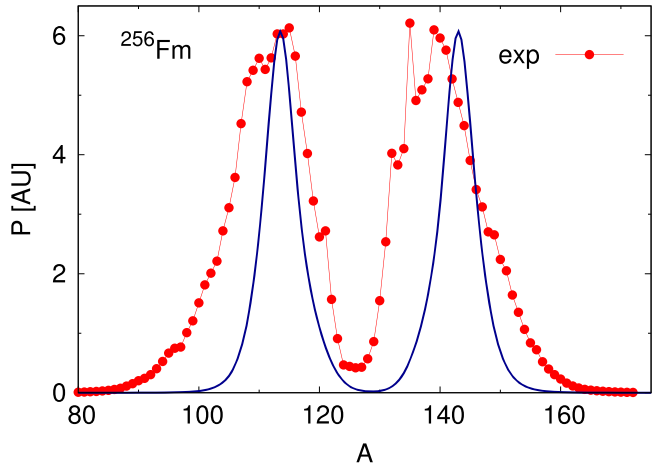

Figure 11. Fragment mass distribution for the spontaneous fission of ^{256}Fm isotope in comparison to the experimental data, taken from [34].

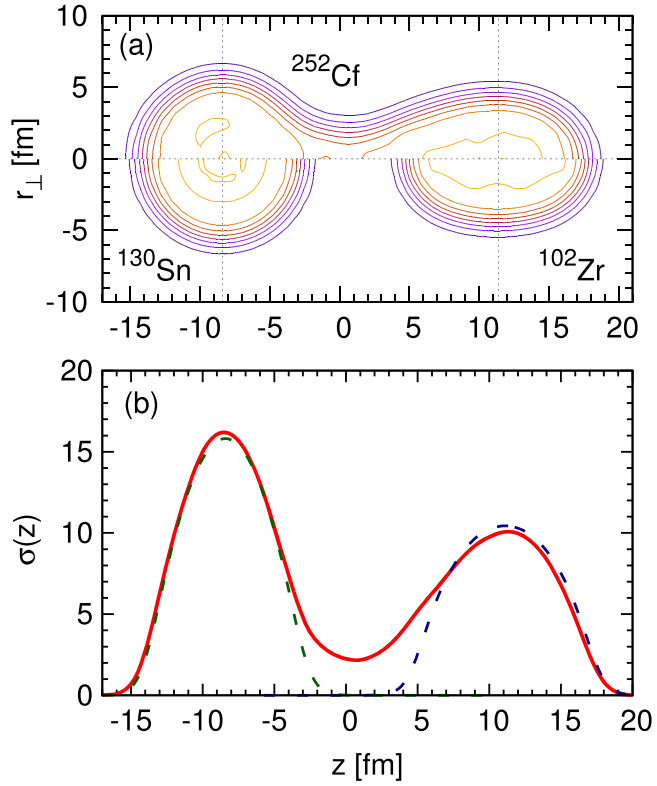

Figure 12. Similar as in figure 5 but for pre-scission configuration of ^{252}Cf (Q_{20} = 217 b, Q_{30} = 66.5 b$^{3/2}$). Density distribution and profiles are compared with ^{102}Zr (Q_{20} = 5.5 b) and ^{130}Sn (spherical).

in figure 11 together with experimental mass yields. The most probable mass of light fragment is reproduced with good accuracy. The heavy fragment peak is slightly shifted in comparison to the experimental one. The broadness of calculated distribution is reduced.

The ^{252}Cf represents nuclei that decay through the asymmetric fission mode (see [29, 30]). In figure 12 the density profile of ^{252}Cf in its pre-scission deformation is shown, as well

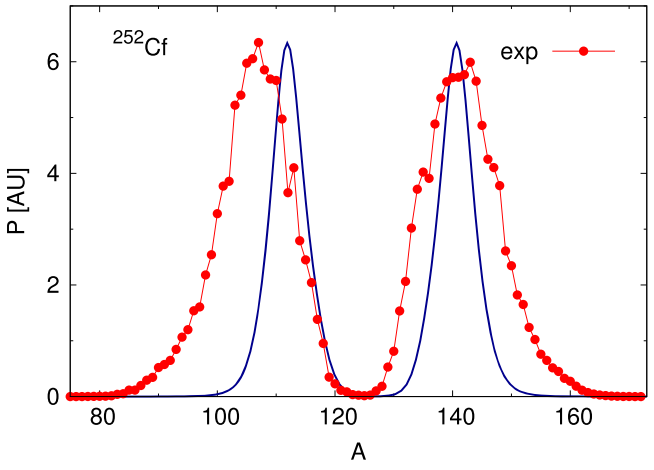

Figure 13. The same as in figure 11 but for ^{252}Cf isotope. Experimental data were taken from [34].

as its linear density function. The fragment mass distribution is presented in figure 13. In this case, the most abundantly produced fission light fragment is not reproduced within the presented method. The predicted mass distribution of the lighter fragment is shifted towards heavier masses in comparison to the experimental data. Probable explanation of these discrepancies comes from the fact, that post neutron emission measurements are presented [34] and average neutron multiplicity is larger in the region of the most probable lighter fragment [35]. Similar to the results of ^{256}Fm, theoretical mass distribution is too narrow in comparison to the observed yield.

The recent experimental studies have brought unexpected observations of β-delayed fission of ^{180}Hg [36, 37]. The most abundantly produced fission fragments have fragment mass asymmetry $A_H/A_L = 100/80$ instead of expected fragmentation leading to two magic ^{90}Zr isotopes. Detailed microscopic analysis [24] explained the dominant character of asymmetric fission valley. The ^{180}Hg, as a product of electron capture in ^{180}Tl, is created with excitation energy not larger than 10.44 MeV. In this nucleus the pre-scission point is in the vicinity of a saddle around 12 MeV above the ground state. Scission point excitation energy should be taken equal to maximal energy available for the nucleus in its ground state. Density distribution in the pre-scission point as well as function $\sigma(z)$ are plotted in figure 14. Fragment mass distribution is compared with experimental data in figure 15. The most probable heavy and light masses (A_H = 100 and A_L = 80) are well reproduced. Calculated yield is too narrow in comparison with the observed one. The peak-to-valley ratio is not reproduced as well.

4. Summary

The presented results confirm that microscopic description of the pre-scission configuration provides a lot of information about physics of fission. Applying the macroscopic method proposed by Brosa to the self-consistently calculated nuclear matter density distribution, we have deduced ambiguous

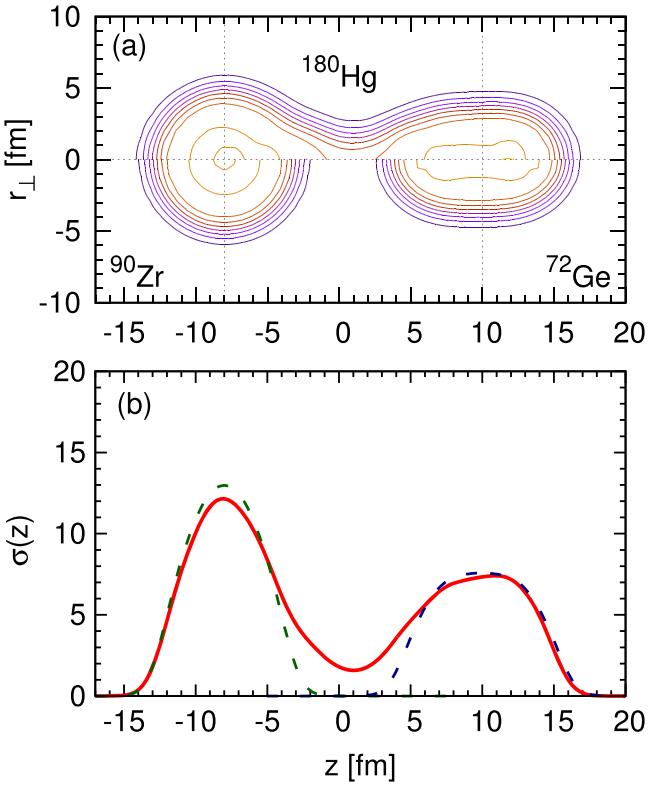

Figure 14. Similar as in figure 5 but for pre-scission configuration of ^{180}Hg (Q_{20} = 130 b, Q_{30} = 30 b$^{3/2}$). Density distribution and profiles are compared with ^{90}Zr (spherical) and ^{72}Ge (Q_{20} = 8 b).

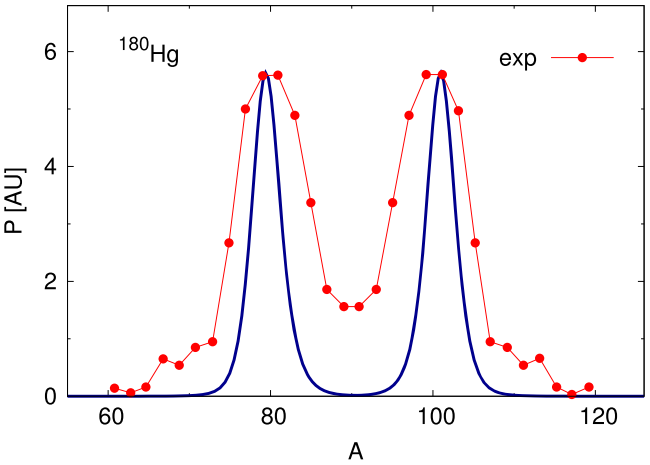

Figure 15. The same as in figure 11 but for ^{180}Hg isotope. Experimental data were taken from [37].

fragment mass yield. The major characteristics of experimentally measured mass distributions, i.e. the most probable masses of heavy and light fragment are reproduced with reasonable accuracy.

The broadness of yields is too narrow as dynamics of the process was omitted in current investigation. The value of temperature used in our studies may also affect the results. Between pre- and post-scission configuration energy usually significantly decreases. In consequence one may assume larger values of excitation energy and temperature, which leads to broadening peaks of mass distribution. In the neck rupture mechanism we have also ignored quantal properties of nucleons, which may impact on fragment mass distribution. We have shown that even in asymmetric fission one of the fragments is close to spherical double-magic nucleus. Strong shell effects in the fragments as well as quantal nature of the neck nucleons may modify the macroscopic model of random neck rupture. All presented distributions, deduced from our static calculations, are much narrower in comparison with experimental ones. Further investigations require inclusion of dynamical effects. It would allow one to reproduce required broadness of mass yields.

Acknowledgments

This work is partially supported by National Science Center in Poland by grant No. 2013/11/B/ST2/04087.

References

[1] Nix J R and Swiatecki W J 1965 *Nucl. Phys.* **71** 1
[2] Wilkins B D, Steinberg E P and Chasman R R 1976 *Phys. Rev.* C **14** 1832
[3] Andreev A V, Adamian G G, Antonenko N V, Ivanova S P and Scheid W 2004 *Eur. Phys. J.* A **22** 51
[4] Andreev A V, Adamian G G, Antonenko N V and Ivanova S P 2005 *Eur. Phys. J.* A **26** 327
[5] Andreev A V, Adamian G G, Antonenko N V and Andreyev A N 2013 *Phys. Rev.* C **88** 047604
[6] Panebianco S, Sida J-L, Goutte H, Lemaître J-F, Dubray N and Hilaire S 2012 *Phys. Rev.* C **86** 064601
[7] Randrup J and Möller P 2011 *Phys. Rev. Lett.* **106** 132503
[8] Randrup J, Moller P and Sierk J 2011 *Phys. Rev.* C **84** 034613
[9] Goutte H, Berger J, Casoli P and Gogny D 2005 *Phys. Rev.* C **71** 024316
[10] Schunck N, Duke D, Carr H and Knoll A 2014 *Phys. Rev.* C **90** 054305
[11] Younes W, Gogny D and Schunck N 2013 *Proc. 5th Int. Conf. on Fission and Properties of Neutron Rich Nuclei (Sanibel Island, FL, USA)* ed J H Hamilton and A V Ramayya (Singapore: World Scientific) p 605
[12] Arimoto Y and Chiba Y 2013 *Phys. Rev.* C **88** 044614
[13] Johansson S 1965 *Nucl. Phys.* **64** 147
[14] http://hal.in2p3.fr/in2p3-00976648
[15] Brosa U and Grossmann S 1983 *Z Phys.* A **310** 177
[16] Brosa U 1988 *Phys. Rev.* C **38** 1944
[17] Brosa U, Grossmann S and Müller A 1990 *Phys. Rep.* **197** 167
[18] Warda M, Egido J L, Robledo L M and Pomorski K 2002 *Phys. Rev.* C **66** 014310
[19] Warda M and Egido J L 2012 *Phys. Rev.* C **86** 14322
[20] Dubray N, Goutte H and Delaroche J P 2008 *Phys. Rev.* C **77** 014310
[21] Berger J F, Girod M and Gogny D 1984 *Nucl. Phys.* A **428** 23c
[22] Egido J L and Robledo L M 2000 *Phys. Rev. Lett.* **85** 1198
[23] Warda M and Robledo L M 2011 *Phys. Rev.* C **84** 044608
[24] Warda M, Staszczak A and Nazarewicz W 2012 *Phys. Rev.* C **86** 24601

[25] Younes W and Gogny D 2011 *Phys. Rev. Lett.* **107** 132501
[26] Decharge J and Gogny D 1980 *Phys. Rev.* C **21** 1568
[27] Berger J F, Girod M and Gogny D 1991 *Comput. Phys. Commun.* **63** 365
[28] Egido J L, Robledo L M and Chasman R R 1997 *Phys. Lett.* B **393** 13
[29] Warda M, Pomorski K, Egido J L and Robledo L M 2005 *J. Phys. G: Nucl. Part. Phys.* **31** S1555
[30] Warda M, Pomorski K, Egido J L and Robledo L M 2005 *Int. J. Mod. Phys.* E **14** 403
[31] Dubray N and Regnier D 2012 *Comput. Phys. Commun.* **183** 2035
[32] Blocki J, Randrup J, Swiatecki W J and Tsang C F 1977 *Ann. Phys., NY* **105** 427
[33] Hulet E K *et al* 1986 *Phys. Rev. Lett.* **56** 313
[34] http://ie.lbl.gov/fission/endf349.pdf
[35] Zeynalov S, Hambsch F J and Obertstedt S 2011 *J. Korean Phys. Soc.* **59** 1396
[36] Andreyev A N *et al* 2010 *Phys. Rev. Lett.* **105** 252502
[37] Elseviers J *et al* 2013 *Phys. Rev.* C **88** 044321